7th National Conference on Computational Mechanics

(MekIT'13)

Trondheim, Norway
13-14 May 2013

Editors:

B. Skallerud
H.I. Andersson

ISBN: 978-1-63266-579-9

On the near-wall vortical structures at moderate Reynolds numbers

Philipp Schlatter*, Ramis Örlü, Georg Eitel-Amor, Qiang Li and Dan S. Henningson
Linné FLOW Centre,
KTH Mechanics, Stockholm, Sweden
e–mail: pschlatt@mech.kth.se

Fazle Hussain
Department of Mechanical Engineering
Texas Tech University, Lubbock, TX, 79409-1021, U.S.A.

Summary In this paper, we study a recent database from direct numerical simulation (DNS) of a turbulent boundary layer (TBL) up to $Re_\theta = 4300$ [Schlatter & Örlü, J. Fluid Mech. 659, 2010] in order to visualise and extract the dominant flow structures in the turbulent near-wall region. In particular, the question of whether distinct hairpin vortices are present close to the wall is addressed. The boundary layer under study is tripped to turbulence, leading to an initial phase of laminar-turbulent transition in which hairpin vortices evolving from classical Λ vortices are the dominant structure of this young turbulent boundary layer. This is in good qualitative agreement with previous experiments and low-Reynolds-number simulations such as Wu & Moin [J. Fluid Mech. 630, 2009]. However, when going to higher Reynolds numbers away from transition, the flow close to the wall is dominated by a staggered array of quasi-streamwise vortices which are similar as observed in earlier channel flow studies. It turns out that even quantitatively, no major differences between boundary layers and channels can be detected; the structures are a few hundred viscous units in length, and slightly inclined [Jeong *et al.*, J. Fluid Mech. 332, 1997]. We also study three-dimensional visualisations of the neighbourhood of regions of strong swirl in planar cuts through the layer (so-called hairpin-vortex signatures), a technique usually applied in experimental studies. However, our 3D views do not reveal clear hairpin vortices. The present results thus clearly suggest that in turbulent boundary layers, hairpin vortices may exist at low Reynolds numbers, induced by laminar-turbulent transition. However, they do not persist in great number the fully developed region. Their dominant appearance as instantaneous coherent structures in the outer boundary-layer region is very unlikely.

Introduction

A significant part of the fuel cost of aeroplanes arises from the frictional drag exerted by turbulent motion within a thin layer directly adjacent to the surface. The influence of viscosity is mainly contained within this turbulent boundary layer (TBL). Notable progress in understanding the involved physical processes has been made to unravel various open questions relating to TBLs, such as scaling with Reynolds number, influence of pressure gradients *etc.*; however, many significant fundamental questions still remain, mostly related to the arising flow structures, and the dominant regeneration processes within the layer.

Experiments and numerical simulations necessarily study idealised boundary layers, evolving on flat surfaces in simplified geometries. In simulations, due to the ease of prescribing boundary and initial conditions, it has been common to study parallel flows such as plane channel flow. However, "real" open boundary-layer flows have been intensively studied both in wind-tunnel experiments and – more recently – also with computer simulations. Of primary interest, as apparent from recent review articles by Marusic *et al.* [30], Klewicki [23], Smits *et al.* [49], and Wallace [57], is the description of turbulent statistics, such as the mean flow and the fluctuation intensities. On the other hand, beyond statistics a suitable description of the boundary-layer flow in terms of coherent vortical structures is important, since it has been used to model wall turbulence, *e.g.* by means of the attached-eddy hypothesis of Townsend [55]. Knowledge of the

dominant structures is paramount, for instance, for designing successful flow-control devices. It is therefore necessary to understand and categorise the three-dimensional composition of the turbulent boundary layer.

Background

From early visualisations it is clear that the turbulent boundary layer is dominated by high intensity velocity fluctuations. For instance, the classical paper by Kline *et al.* [25] included hydrogen-bubble visualisations that lead the authors to conclude that the near-wall flow is organised in a streaky pattern with alternating higher and lower streamwise momentum, spaced at the spanwise length scale of about 100 viscous units $\ell_\star$. All subsequent measurements and simulations confirmed these streaks as a very robust feature, essentially independent of the flow Reynolds number (Re) [24]. The streaks play a critical part in the dynamics and turbulence regeneration by sustaining the turbulent production in the buffer layer. However, what processes really go on in the buffer layer has been extensively studied using a number of different techniques and model problems [12, 56], identifying a self-sustaining process based on a recurrent (linear) instability followed by nonlinear breakdown of the near-wall streaks (see the review by Panton [36]). Schoppa and Hussain [47] showed that most streaks are indeed stable, but can sustain transient growth leading to formation of nearly streamwise vortices, and that spanwise (sinuous) oscillations of the streaks were responsible for triggering the transient growth. These quasi-streamwise vortices agreed well with those actually identified in simulated turbulent channel flows at comparably low Reynolds numbers [19].

Besides confirming the existence of the turbulent streaks as fundamental structures in wall-bounded turbulent flows, "there has been considerable controversy as to the existence of hairpin vortices" [29]. Conceptually introduced by Theodorsen in 1952, the hairpin structure "represents the universal element of the structure of turbulent flow" and "consists simply of a vortex bundle or tube attached to the wall [...] forming a loop or horseshoe extending into the boundary 'layer' " [52]. To illustrate a generic hairpin vortex, a visualisation of a few clear examples taken from numerical simulations is included in Fig. 1, obtained at comparably low Reynolds number. In a very similar way, the early experimental visualisation presented by Head and Bandyopadhyay [13] provided "strong experimental evidence for their ubiquitous nature" [49] and remains "perhaps the strongest experimental support for the existence of hairpin vortices in the logarithmic layer" [2]. In addition to the complete, *i.e.* fully symmetric, hairpin vortices, which "exist and play some role in the dynamics of turbulence production" [40], non-symmetric incomplete variants (denoted "hooks" or "canes") have been found in the analysis of the direct numerical simulation (DNS) data of Spalart [50] by Robinson [40], who "proposed an idealized model for low-Reynolds number boundary layers" in which "quasi-streamwise vortices dominate the buffer region, while arch-like vortices are the most common vortical structure in the wake region", and a mixture of both exist in the overlap region "often as elements of the same vortical structure".

While the work by Head and Bandyopadhyay [13] appears to be the clearest experimental evidence for the existence of hairpin vortices in the near-wall region of turbulent flows, considerable work has followed in particular motivated by the advances made in particle-image velocimetry (PIV). In this respect, Adrian [3] was probably the first to extract planar quantitative information about hairpins. Based on the idea that hairpin vortices most often occur in spatially coherent packets which originate from the near-wall region and grow upwards in a ramp-like arrangement, the concept of "hairpin vortex signatures" (HVS) was introduced by Adrian [3] characterising the flow elements that *would be seen* when cutting through the afore-

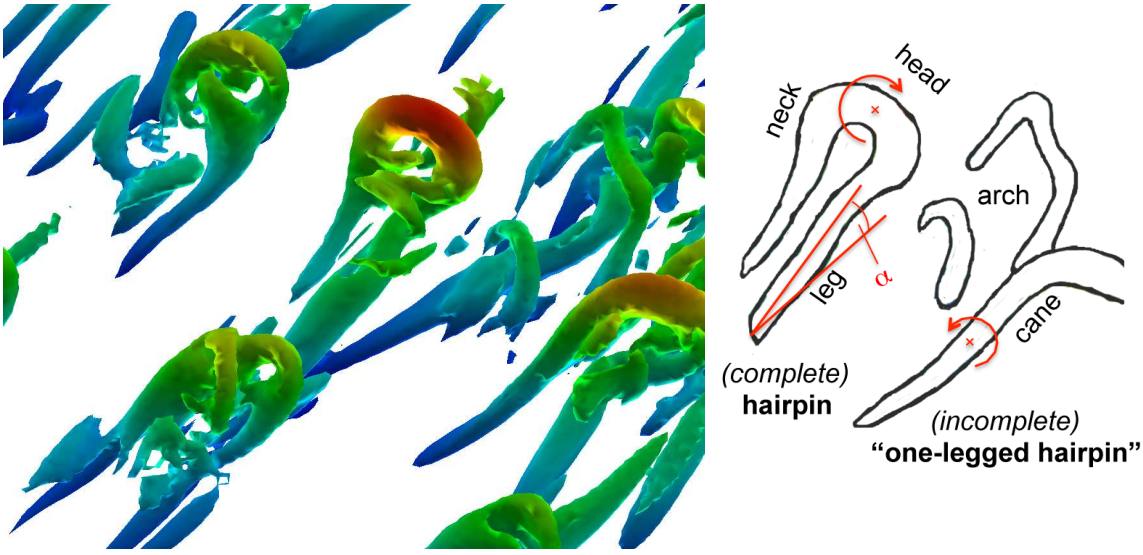

Figure 1: *Left:* Visualisation of hairpin vortices in a turbulent boundary layer, $Re_\theta \approx 500$, isocontours of negative λ_2 [18] coloured by the streamwise velocity, ranging from low (blue) to high (red). The incipient appearance of secondary (offspring) vortices can be seen, similar to a re-generation processes [64]. Flow from lower left to upper right. *Right:* The conceptual sketch of hairpin vortices with their constituting parts; individual arches and cane.

mentioned arrangement. A large body of statistical evidence has been supplemented for HVS by means of PIV [7, 54] extending even to atmospheric boundary layers at very high Reynolds numbers [14]; some, however, “without clear signs of coherent hairpin vortex motions” [31]. “Stereoscopic PIV measurements, on planes inclined both with and against the principal vorticity axis of a proposed hairpin model” [16], were followed by a number of articles [10, 16] and constitute an effort to draw conclusions about the three-dimensional structures, which instantaneously “would appear to be closer to the asymmetric cane-type structures observed by (among others) Robinson (1991)” [16]. Direct observations of the three-dimensional coherent structures in turbulent boundary layers have become possible very recently through tomographic PIV: Instantaneous three-dimensional velocity volumes, be it at low [48] or high [9] Re, have been found to be predominantly populated by one-sided hairpin legs and canes or asymmetric (cane type) vortices, respectively. However, it remains unclear if the spatial resolution of these methods was sufficient for drawing these conclusions.

Although the amount of evidence for the existence of hairpin vortex signatures, *i.e.* indirect evidence for hairpins, is overwhelming, “the observations are constrained to two dimensions, and use fields of view which are too short to observe the large-scale organization of the overlap region” [8]. Hence it would appear natural that DNS is the tool of choice to dissect and educe the near-wall kinematics and dynamics. Nonetheless, early DNS investigations [40] have not yielded dominant complete hairpin vortices, but rather cane-type vortices. This observation, in the near-wall region, is in line with the quasi-streamwise vortices [19, 47]. The disparity between experiments and simulations has largely been unresolved, and attributed to aspects such as Re difference, artificial periodicity imposed in the numerical domains versus the spatially-developing character of the real-world boundary layers, resolution issues, *etc.* Nevertheless, there has been considerable progress in that direction, but so far most simulations have been obtained in channels. Regarding the evolution of hairpin vortices in channel flows, the so-called

parent-offspring mechanism has been suggested as being active in the near-wall region. For instance, Zhou *et al.* [64] show in their simulation that an initial hairpin vortex quickly generates other hairpins which "align coherently in packets [...] forming the LSMs, and then the packets align coherently to form the very large-scale motions" [22].

A pivotal point regarding the visualisation of vortical structures in boundary layers is the DNS by Wu and Moin [59], which "provides, for the first time, clear evidence of the quantitative shapes of individual hairpin vortices", that are — as Marusic [28] remarks in his featuring *Focus on Fluids* paper — "surprisingly [...] remarkably symmetric" and "corroborated their unambiguous and densely populated presence in boundary layers" [49]. The fact that "such a direct evidence for their dominance has not been reported in any numerical or experimental investigation of turbulent boundary layers since the flow visualization experiments of Head and Bandyopadhyay [13]" led Wu and Moin [59] to denote this as the "forest of hairpins" foreseen by Perry and Chong [37]. Even though the paper by Wu and Moin [60] initially emphasised the concern that "the persistence of the present hairpin forest into higher Reynolds number regions [...] require[s] further investigation": Hairpin vortices are quite common structures in various types of transitional flows, for instance also in classical K and H-type transition. A hairpin vortex, once created by transitional mechanisms such as *e.g.* wall-normal shear-layer roll-up [41] or varicose streak instabilities in bypass transition [4], will survive and advect downstream for a while until they are affected by viscosity or other (stronger) dynamics in the layer.

The fact that the simulation domain of Wu and Moin [59] ended very close to the point of laminar-turbulent transition — in their case initiated via travelling patches of free-stream disturbances — has been suspicious to other researchers. Nonetheless, the same authors observed later on, based on their extended Re-range going now up to $Re_\theta = 2000$ instead of 900, "that the preponderance of hairpin vortices in the turbulent boundary layer is not simply a result of the decayed remnants of the upstream transitional hairpin forest" [58] and that the "persistence of hairpin forests [goes] up to Re_θ=1900" [61]. Compared to the visualisation of the forest of hairpins in the low Re DNS [59, 60], the snapshots at their higher Re [61, 62] are however much more chaotic and it appears difficult to unambiguously identify a clear forest of hairpins, even though the authors state that their "DNS results demonstrate, beyond reasonable doubt, a preponderance of hairpin vortices in ZPGFPBLs up to momentum-thickness Reynolds number 2000" [62]. On the other hand, even this evidence does not go beyond $Re_\theta = 2000$ which is still a low Reynolds number from a practical point of view.

Despite these re-affirmations, the most recent review on this topic by Marusic and Adrian [29] admits that the "evidence for packets at high Reynolds number is less detailed" and as indicated by Marusic [28] "considerable activity is likely to follow in light of the results reported by Wu and Moin". The present paper summarises some results from one of these activities that addresses not only the question whether hairpin vortices or packets are dominant, representative for or even existent in wall turbulence, but also tries to bring together the different views deduced from planar fields as *e.g.* extracted from PIV experiments. Results from activities in the same direction have for instance been reported by Jiménez *et al.* [20] who finds it "difficult [...] to describe the [observed] structure[s] [...] as an ordered hairpin forest", while Pirozzoli [38] observes "that the near-wall region is mainly populated by quasi-streamwise vortices, whereas hairpin-shaped vortices are the statistically dominant pattern in the outer layer, even though canonical hairpin-shaped vortices are rarely seen in instantaneous flow realizations, and asymmetric, cane-shaped vortices are far more frequent [51]."

Approach

Only during recent years it has become possible, largely due to the increased availability of large-scale computer resources, to simulate truly spatially developing boundary layers reaching up to reasonably high Reynolds numbers. As demonstrated by Schlatter *et al.* [46], such simulations can be initiated with a laminar Blasius inflow plus a numerical version of a trip wire, essentially including the whole laminar-turbulent transition process in the simulation domain. After transition, the boundary layer adapts and approaches a fully-developed turbulent state. In the mentioned reference, excellent agreement with experiments performed in the MTL (Minimum-Turbulence-Level) wind tunnel at KTH Stockholm could be obtained at a Reynolds number $Re_\theta = 2500$, based on the momentum thickness θ and free-stream velocity U_∞. Later, this DNS has been extended in length, width and height, to reach an even higher Reynolds number $Re_\theta = 4300$ [44]. Again, excellent agreement with experiments could be ascertained, as documented by Örlü and Schlatter [35]. Thus, this database can be used as a valid basis for an analysis of the vortical structures in wall turbulence. The underlying simulation does not contain any effects of periodicity since a truly spatially developing boundary layer is simulated without any recycling or rescaling, and the Reynolds numbers are high enough to ensure that the state is far from the transitional region. Furthermore, due to extensive comparison with experiments, one can be confident that the setup of the problem (tripping, pressure gradient, domain size *etc.*) is a true realisation of a fully developed turbulent boundary layer.

The major difference between the simulation by Wu and Moin [59] and the ones by Spalart [50] (analysed by Robinson [40]), Jiménez *et al.* [20] or Pirozzoli *et al.* [38] is the streamwise peridocity and the different prescription of the inflow and boundary conditions, *i.e.* recycling and recycling-rescaling, respectively. This point has been suspected by Wu and Moin [59] as the "primary reason that previous simulations did not see this dominance [of hairpins]", hence "how, or if, these structures relate to the simulation scheme and the prescription of the inflow and boundary conditions will need to be resolved" [28]. Since the simulations by our group [46, 44], more than doubling the highest Re_θ of Wu and Moin [61], go through natural transition the examination of the present DNS dataset is most suitable and not susceptible to "the primary reason" brought forward by the above cited references.

In the following, we will briefly summarise our results on the extraction of hairpin vortices from the simulation database. First, details of the DNS and the numerical techniques are discussed, including the fringe-region technique and the turbulence tripping. Then, we summarise relevant statistical data obtained from the simulation evincing the fully developed turbulent nature of the near-wall turbulence as well as documenting the interplay between outer and inner layer. The heart of the paper follows, in which we present and justify our various eduction and visualisation schemes; including three-dimensional flow visualisations, hairpin-vortex signatures, and a method based on conditional averages.

Simulation Setup

We study a spatially developing turbulent boundary layer under zero pressure gradient (ZPG). In order to be as close as possible to naturally developing boundary layers, we chose a numerical domain with laminar Blasius profile as inflow. As discussed above, transition to turbulence is then initiated inside the domain. Further details of the present calculations are given in Schlatter and Örlü [44]. The influence of the tripping and its parameters on the evolving flow is summarised in our recent article [45]. An initial large-eddy simulation of the same domain and setup, but with reduced spatial and temporal resolution, was also performed, and these simula-

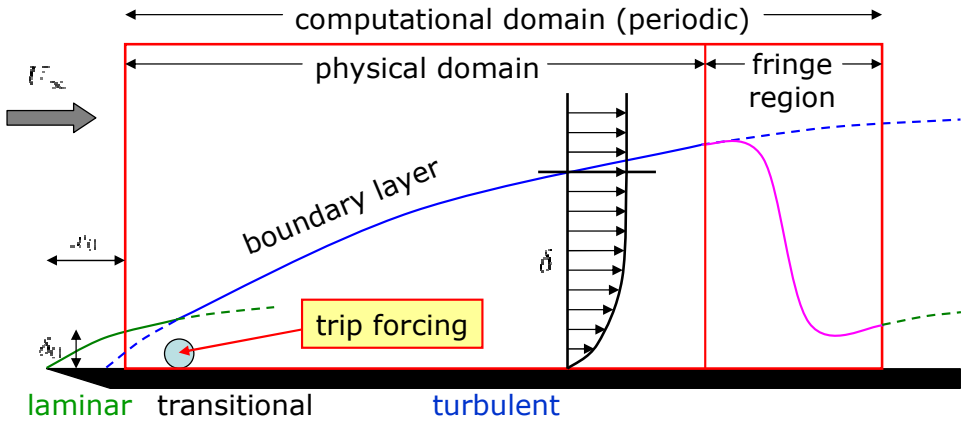

Figure 2: Sketch of the numerical domain, including fringe region and location of the tripping. The inflow is laminar with a finite boundary-layer thickness $Re_{\delta_0^*} = 450$. The fringe region is located at the downstream end of the domain to enforce periodic boundary conditions in the streamwise direction.

tion results were carefully compared and verified with respect to other existing data [43].

A fully spectral method is used to solve the three-dimensional, time-dependent, incompressible Navier–Stokes equations [6]. In the wall-parallel directions, Fourier series with dealiasing are used, whereas the wall-normal direction is discretised with Chebyshev polynomials. Time is advanced with a standard mixed Crank–Nicolson/Runge–Kutta scheme. The boundary conditions in the freestream are of Neumann type, *i.e.* the wall-normal variation of the velocity components is assumed zero at the upper boundary. This requirement together with incompressibility leads to a constant mean streamwise velocity at the upper boundary, whereas the normal velocity component might be non-zero to account for the boundary-layer growth.

A Fourier discretisation requires the underlying flow solution to be periodic. The imposed spanwise periodicity does not pose any difficulty. However, a spatially developing boundary layer is obviously not periodic in the streamwise direction. The required periodicity is made consistent with the spatially developing nature of the problem by adding a so-called "fringe region" at the end of the domain, see the sketch in Fig. 2. In the fringe region, the outflowing fluid is forced via a volume force to the laminar inflow Blasius profile, located at $Re_{\delta_0^*} = 450$ based on the displacement thickness δ_0^* at the inlet.

We would like to emphasise that the use of the fringe method together with periodic boundary conditions on the *computational domain* does not imply any periodicity within the *physical domain*. For the latter, the inflow is laminar Blasius flow without fluctuations, and the outflow can be considered similar to a convective condition supplemented with a sponge region. The fringe region is an entirely numerical technique to adapt the Fourier spectral method to non-periodic domains, and is completely unrelated to the physical setup of a spatially developing boundary layer. In that regard, the present simulation setup is fundamentally different from the (pseudo-)periodic simulation by Spalart [50], or fully periodic channel-flow simulations. The present setup is however equivalent to the setup of Wu and Moin [59], albeit using a higher-order discretisation in the present case. Thus the vortical structures found in the present data cannot be attributed to any residual effect of periodicity.

The computational domain is $x_L \times y_L \times z_L = 6000\delta_0^* \times 200\delta_0^* \times 240\delta_0^*$ with $8192 \times 513 \times 768$ spectral modes in the streamwise, wall-normal and spanwise directions, respectively; the num-

ber of points on the finer physical-space mesh is a factor of 1.5×1.5 larger in the wall-parallel direction due to the dealiasing. The height of the computational domain is chosen to be at least 2.5 times the largest 99%-boundary-layer thickness δ_{99} at its maximum; in the spanwise direction an even larger domain is chosen to ensure the correct development of large-scale structures scaling in outer units. The maximum grid spacing in viscous units in the three directions is $\Delta x^+ \times \Delta y^+_{\max} \times \Delta z^+ = 9 \times 8 \times 4$, typical of well-resolved simulations of wall turbulence. The numerical code is fully parallelised using the message-passing interface (MPI) running on $\mathcal{O}(4000)$ processors.

Apart from the mentioned boundary-layer cases, a number of results pertaining to channel flow are also included. The same simulation code [6], albeit without fringe forcing, has been used to simulate standard periodic channel flow. The flow was given sufficient time to adapt such that any potential transient effect due to the specific initial conditions were long forgotten. Statistics from these simulations are in perfect agreement with the literature, and have been used in other studies as well, *e.g.* Ref. [27]. Since fully resolved channel flow can be considered fairly standard, even at Reynolds numbers $Re_\tau = 590$ based on the friction velocity u_τ and channel half height h, no further explanations or validation are necessary.

Turbulent Statistics and Characterisation

Selected turbulent statistics of the simulation data base are now discussed to give an overview of the available data and to affirm the reader that the used simulation data is indeed representative of a fully developed turbulent boundary layer. The streamwise development of skin-friction coefficient c_f, wall pressure fluctuations p^+_{rms} and wall-shear stress fluctuations τ^+_{rms} are shown in Fig. 3, with rms denoting root-mean-square. These quantities serve as a quantification of the streamwise development of the boundary layer in the near-wall region [45]. The tripping employed for the present data leads to rapid transition close to the numerical inlet, with a minor (but well-known [4]) overshoot above the turbulent correlation. The data by Wu and Moin [61] shows later and more gradual transition in agreement with other studies of bypass transition [4]. As discussed by Schlatter and Örlü [44], in particular τ^+_{rms} provides a convenient quantification of the inner-layer convergence of the flow. The agreement with the DNS data from other recent boundary-layer simulation [20] is very good. However, compared to the DNS data from Wu and Moin [61], the predictions of both τ^+_{rms} and p^+_{rms} are quite different from the present results: τ^+_{rms} is about 5-10% higher than the present DNS for the whole Reynolds-number range, while the pressure fluctuations p^+_{rms} are below the present data. The cause of this difference is unclear; however, the present data is consistent with experiments and other (channel and TBL) simulations [34]. At the same time, it is interesting to link this observation, *i.e.* high τ_w and low p fluctuations, to the preponderance of hairpin vortices ("wall signatures of hairpin packets") [53] as *e.g.* studied by O'Farrell [32]. Even though a direct influence of these discrepancies on the vortical structures in the boundary layer further away is unlikely, differences of that order for fully resolved DNS are quite remarkable, and can only to some extent be explained by the tripping procedure [45].

A comparison of the mean streamwise velocity and turbulence intensity profiles with experimental data [33] and simulation data [20] at various Re is shown in Fig. 4. The difference between the two DNS data sets at $Re_\theta = 1968$ is negligible, indicating that — given the quite different ways the two simulations were initiated and the diverse numerical methods — the boundary layer has reached a fully-developed state. In addition, the agreement for higher Reynolds numbers $Re_\theta = 2500$ and 4300 is also excellent.

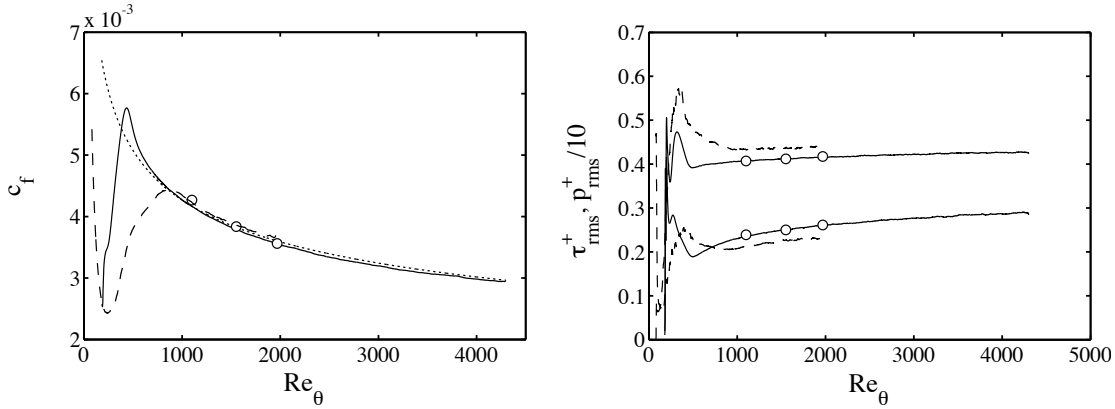

Figure 3: Streamwise evolution of the skin-friction coefficient c_f, wall pressure fluctuations $p^+_{\rm rms}$ and wall-shear stress fluctuations $\tau^+_{\rm rms}$. ——present DNS, - - - -DNS from Ref. [61], ∘ DNS from Ref. [20], ····· $c_f = 0.024 Re_\theta^{-0.25}$. Left: c_f, right: $\tau^+_{\rm rms}$ and $0.1 \cdot p^+_{\rm rms}$; pressure fluctuations are the lower set of data.

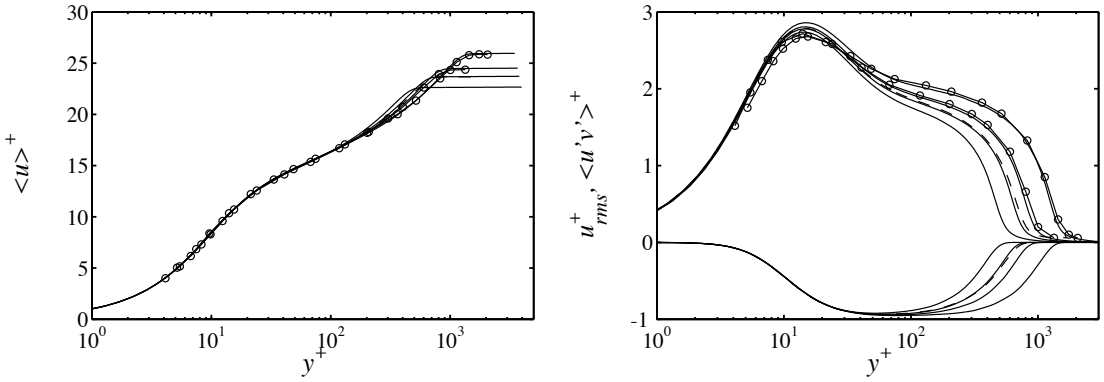

Figure 4: Comparison of the mean streamwise velocity profile and turbulent fluctuations as a function of wall distance y^+ at $Re_\theta = 1410, 1968, 2526, 4071$. ——present DNS, ∘ experiments from Ref. [33] and partially presented in Ref. [46] at $Re_\theta = 2526, 4071$. - - - -DNS from Ref. [20] at $Re_\theta = 1968$.

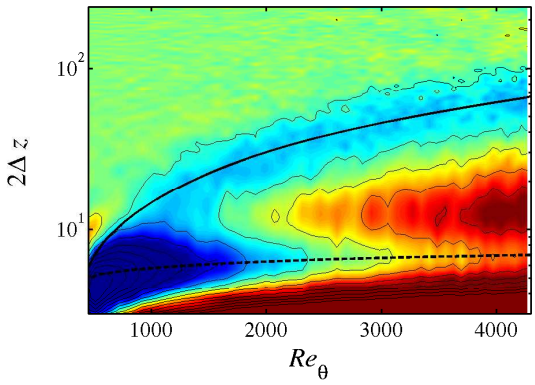

Figure 5: Contours of the spanwise two-point correlation of the wall shear stress $R_{\tau\tau}$ as a function of the downstream distance measured as Re_θ. The separation is measured in units of the inlet displacement thickness δ_0^*. ——— corresponds to $0.85\delta_{99}$ and - - - - to 120 plus units. Colours range from $R_{\tau\tau} = -0.06$ (blue) to +0.06 (red).

Considering solely the mean velocity and the fluctuation profiles naturally does not give any insight into the spatial scales of the turbulent motions. One way the complex interplay of at least two dominant spatial sizes can be studied is by considering a contour map of the spanwise two-point correlation of the wall shear stress $R_{\tau\tau}$ as shown in Fig. 5. Such a visualisation shows the dominant spacing and size of turbulent eddies detectable at the wall [46]. $R_{\tau\tau}$ is unity at zero separation $\Delta_z = 0$, followed by a first minimum, indicating the most probable spacing for small structures. This negative peak at about $2\Delta_z^+ \approx 120$ reflects the spacing of near-wall streaks. This first minimum is followed by a clear maximum at twice this distance. Another negative peak, scaling as $2\Delta z \approx 0.85\delta_{99}$ is clearly visible for higher Re_θ, indicating the footprint of large-scale (*i.e.* wide) structures onto the fluctuating wall-shear stress. As discussed for instance by Hoyas and Jiménez [15] and Örlü and Schlatter [34] it is exactly this growing outer-layer influence onto the near-wall region that gives rise to subtle Re effects close to the wall, *e.g.* the slowly rising maximum of the streamwise fluctuation $u_{\rm rms}$ or of $\tau^+_{w,\rm rms}$ with increasing Re_θ. Note that a clear separation between the two different scales is possible only for $Re_\theta > 1500$; below that Reynolds number essentially one wider spectral peak occurs indicating very similar scales for both inner and outer motions.

Two-Peak Structure

It has become customary to plot premultiplied spectra when assessing spectral information in wall-bounded flows. Note that the reason for premultiplying with the wavenumber is solely to directly allow a comparison of the total energy content within a certain wavenumber range, when plotting along a logarithmic axis. The two-peak structure in Fig. 6, as already seen right at the wall in Fig. 5, is clearly present throughout the boundary-layer height. The inner peak, related to the near-wall streaks, is virtually independent of Reynolds number. As expected, measuring at higher Re gives rise to an increasingly pronounced outer peak, located at a spanwise width of about one boundary-layer thickness δ_{99}, and a wall-normal location of $0.4\delta_{99}$. These results are consistent with experimental results at higher Reynolds numbers, see *e.g.* Ref. [17], and other numerical simulations. Note, however, that there are quantitative differences of the outer-layer characteristics compared to channels, in particular related to the spanwise width and spectral energy of the outer structures [20].

The interplay between outer and inner layer can also be appreciated by considering a thin streamwise slice of the boundary layer, as shown in Fig. 7. Here, the boundary layer is vi-

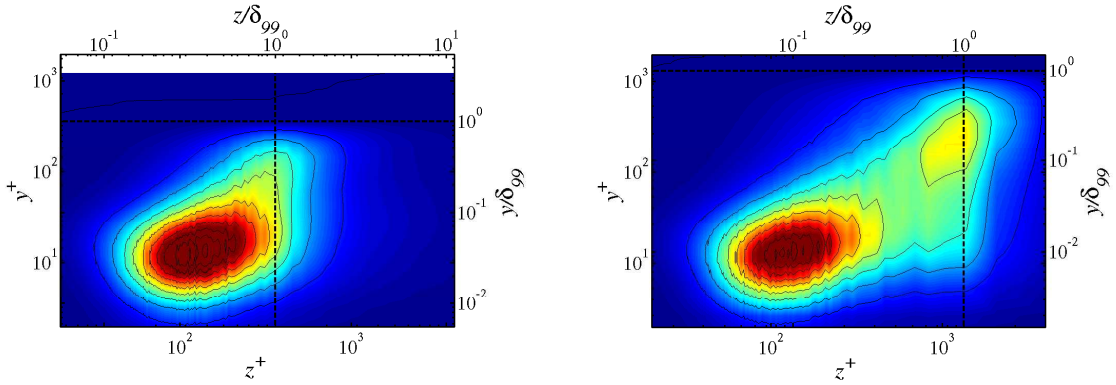

Figure 6: Premultiplied spanwise spectrum of the streamwise velocity component at $Re_\theta = 1000$ ($Re_\tau = 360$, left) and $Re_\theta = 4300$ ($Re_\tau = 1350$, right), scaled with u_τ^2. ----corresponds to $1.0\delta_{99}$ both in spanwise and vertical direction. Colours range from 0 (blue) to 2.5 (red).

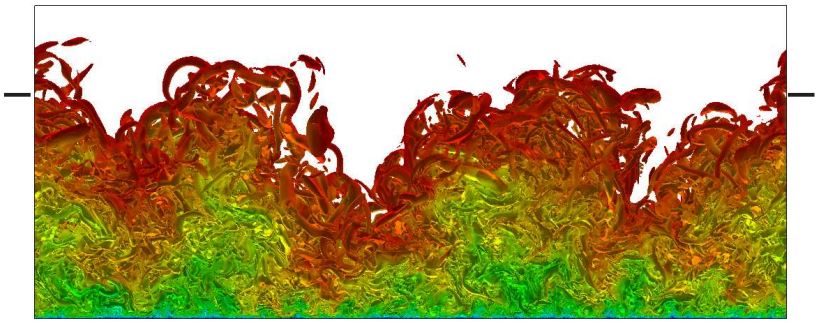

Figure 7: Instantaneous snapshot showing a frontal view of a thin slice ($\Delta x^+ \approx 1000$) of the boundary layer at $Re_\theta \approx 4000$. Isocontours of $\lambda_2^+ = -0.00046$ coloured with the total streamwise velocity u ranging from 0 (blue) to 1 (red). The mean δ_{99} is indicated by the thick solid lines on the sides.

sualised by means of isocontours of negative λ_2, a criterion designed to identify vortices [18] explained further below. As well known, the (instantaneous) edge of the boundary layer, roughly defined as the interface between the rotational and irrotational flow, features deep valleys; their distances scaling in outer units. However, what makes this view specifically illustrative is the fact that the regions with low-speed outer structures correspond to a locally thick layer. Conversely, the boundary layer is compressed in the other regions, making the previously mentioned amplitude modulation of the near-wall structures intuitively clear.

Vortical Structures

In this section, databases for turbulent boundary-layer and channel flows are analysed to educe and identify the dominant vortical structures. We begin with a description of the adopted eduction methodology [19], before we present the vortical structures obtained for the different flow regimes, *i.e.* distance from transition, and compare them to structures educed in (periodic) channel flow. As a side note, an animated three-dimensional visualisation of the boundary-layer data is contained in an article available online at arXiv [42], showing the streamwise development of the vortical structures.

Eduction Scheme

Unfortunately, there does not exist a single unambiguous definition of a vortical coherent structure. We therefore follow previous works by defining a coherent vortical structure as a connected region of fluid undergoing swirling motion with the same sense of rotation around a common vortex axis. Based on the thorough discussion of various identification schemes in Jeong and Hussain [18] we employ here the λ_2 criterion to identify vortices proposed in the mentioned reference: Given the symmetric and antisymmetric components of the velocity gradient tensor, S_{ij} and Ω_{ij}, the scalar quantity λ_2 is defined as the second (middle) eigenvalue of $S_{ik}S_{kj} + \Omega_{ik}\Omega_{kj}$. A certain point in space is part of a vortex if $\lambda_2 < 0$. Other single-point criteria, such as the swirling strength or the Q criterion are popular choices, are possible, however we are convinced that the present results are not dependent on the choice of the single-point measure. Note that λ_2 is not dimensionless, so it has to be appropriately scaled.

The present vortex-eduction scheme for coherent structures is similar to the one used by Jeong *et al.* [19] based on the λ_2-criterion. The basic underlying idea is the observation that the region of the most intense appearance of vortices, the buffer layer, is dominated by quasi-streamwise vortices. It is now assumed that any dominant coherent structure is necessarily connected to these quasi-streamwise vortices in the near-wall region, irrespective of whether or not these vortices are independent coherent structures or part of larger constructs such as hairpin vortices. As further detailed below, the streamwise vortices are expected to be in a region $y^+ < 40$ from the wall; also certain constraints regarding their length and streamwise orientation will be made.

Other methods for identifying vortices based on velocity signals such as VITA (variable interval time average), Q2 and Q4 conditional sampling, *etc.* suffer from the fact that the educed structures are expected to be more smeared than those using λ_2-criterion, thus it is more difficult to define a sharp boundary of the entire structure [19].

The eduction scheme is divided into the following four basic steps, which are applied to individual instantaneous three-dimensional velocity fields: i) detection of the vortex core of each quasi-streamwise vortical structure, regardless of the sense of rotation. For this purpose, local minima of λ_2 in the region $10 < y^+ < 40$ in each $y - z$ plane are extracted. Lines connecting these local minima in successive $y - z$ planes are then considered to be vortex cores if the

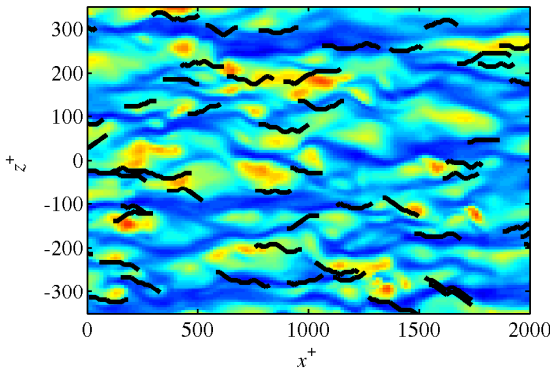

Figure 8: xz plane close to the wall ($y^+ = 15$) showing the extracted vortex cores (black) superimposed onto a colour rendition of the streamwise velocity. Extracted from the turbulent boundary layer, $Re_\theta \approx 3500$.

following two additional conditions are fulfilled: *a)* the streamwise length of the vortex core is at least 150 wall units; *b)* the inclination and tilting angles of the vortex core with respect to the streamwise direction x are within ± 30 degrees. Inclination and tilting angles denote the angles in the streamwise/wall-normal and streamwise/spanwise planes, respectively. ii) a three-dimensional window of about $360 \times 100 \times 160$ viscous units is selected centred around the midpoint (or alternatively the headpoint) of each extracted vortex core. iii) an average of the three-dimensional velocity field within the various chosen windows from each educed vortex core with the same sense of rotation is constructed; the necessity to take the sense of rotation into account is discussed below. iv) Based on this ensemble-averaged velocity field, the educed vortex structure can now be obtained by once again computing the λ_2 scalar field based on the conditionally averaged velocity field. With regards to point iii) it is important to recall, as already discussed by Johansson *et al.* [21], that symmetric averaged patterns can be the result of the spanwise flow homogeneity. Therefore, it is necessary to include in the average only streamwise vortices with the same sense of rotation. For vortices with opposite rotation sense, a mirrored velocity field can be considered in order to preserve the spanwise asymmetry in the average. Eventual vortex heads (spanwise oriented vortices) do not change their direction due to mirroring. Similar precautions have *e.g.* been taken by other studies [11, 19]. The mirrored structures can subsequently be added to the total average in order to increase the sample size.

As an illustration of steps i)–iii), *i.e.* the selection of the relevant streamwise vortices, Fig. 8 shows an excerpt of size 2000×700 viscous units of the boundary layer. On average, such an area is populated by 40 identified vortices, with the area for each vortex (in plus units) to be approximately 200×200.

By construction, the scheme is designed to eliminate ambiguities such as multiple detections of one single structure, the detection of different parts of different structures, and detection of different types of structures. The quality of the average can be improved in several ways, *e.g.* by allowing slight shifts in the wall-parallel directions of the individual realisations, as discussed in Jeong *et al.* [19]. For the present work, however, it turned out that even without this additional adjustment step the quality of the average was sufficient.

Transitional Phase

We begin our analysis of the boundary-layer data close to the tripping location. An instantaneous visualisation in the region $Re_\theta = 300$ to $Re_\theta = 500$ is shown in Fig. 9. The visualised region only contains about 5% of the total length of the computational domain. The initial development

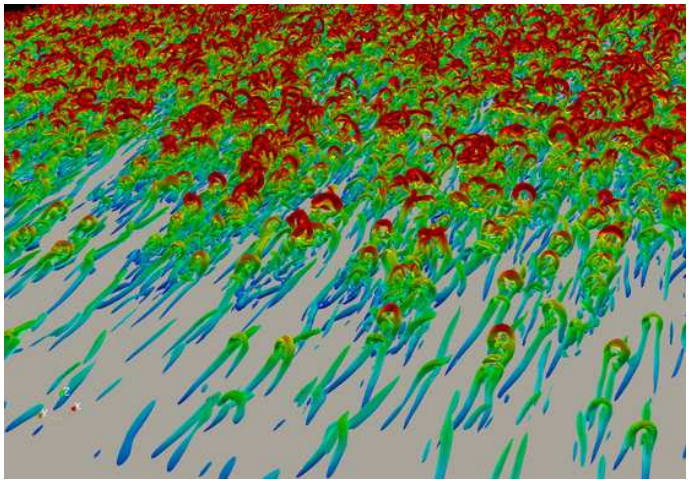

Figure 9: Instantaneous snapshots showing a three-dimensional visualisation of the vortical structures at $Re_\theta = 300$. Isocontours of negative λ_2 identifying vortical structures are coloured by the wall distance. Clearly, transition to turbulence is characterised by the appearance of Λ and hairpin vortices. At later stage, the hairpin vortices are the dominant coherent structures as a remnant of transition. Contour levels: $\lambda_2^+ = -0.0084$.

of the boundary layer can be clearly seen: Laminar-turbulent transition (Fig. 9) is induced by the trip forcing as described above. The subsequent breakdown to turbulent flow is characterised by firstly the appearance of velocity streaks and secondly by unambiguous hairpin vortices, which are seen to dominate the whole span of the flow. The origin of the first hairpins is clearly in the specific tripping chosen for this case. Nevertheless, the hairpin vortices increase in number, and individual distinctive heads of such vortices are clearly visible for some distance downstream (Fig. 9) at $Re_\theta = 500$. This feature of post-transitional or low-Re turbulent flow is — in our view — the one observed in the study by Wu and Moin [59], there denoted as "forest of hairpins". Note also the striking similarity of the structures seen in Fig. 9 to those shown by Head and Bandyopadhyay [13]. We can thus visually confirm the results by Wu and Moin [59], *i.e.* that hairpins are indeed the dominant structure in a near-transition turbulent boundary layer.

Extending the visual evidence presented in Fig. 9, it is now interesting to analyse whether the vortex-eduction method described above is able to extract a dominant coherent structure resembling the hairpin-type vortices. Using two uncorrelated velocity fields the algorithm restricted to the early region, $Re_\theta \approx 200 \sim 400$, identified a total of 189 unambiguous vortex legs satisfying the conditions listed above. A rendering of the three-dimensional ensemble-averaged vortex structure obtained from a subset of these 189 legs is given in Fig. 10. The alignment of the structures was done, as opposed to the turbulent cases described further below, at the head points of the structures to account for the potentially different lengths of the legs of the structures; these head points also define the coordinate system origin used in the plot. As shown in Fig. 10, the average structure occupies an area of about 250×80 viscous units, using the values of u_τ slightly downstream in the (unambiguous) turbulent region at $Re_\theta = 650$ or $Re_\tau \approx 200$. The main educed body of the structure is a quasi-streamwise vortex, reaching from very close to the wall ($y^+ \approx 10$) to a maximum distance of $y^+ \approx 80$ at the downstream end. Interestingly, the averaged structure does not only contain one vortex, but also a second leg. A counter-rotating but essentially parallel tube is detected at a spanwise distance of about 50 viscous units. The two tubes are connected via a visible bridge. The two legs together with their connection can readily be interpreted as a hairpin vortex. The corresponding velocity field naturally features a

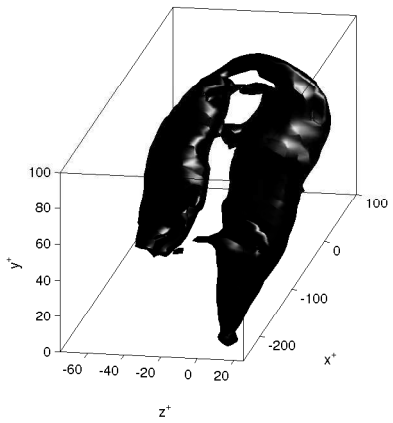

Figure 10: Educed hairpin vortex in the early transitional region ($Re_\theta \approx 200 \sim 300$) over 14 clear hairpin structures. Isocontour level of $\lambda_2^+ = -0.0035$, calculated based on the shear stress at $Re_\theta = 650$.

strong low-speed streak between the legs of the hairpin, together with a characteristic "kink" at the position of the head. Note that the smeared appearance of the vortex head (or bridge) is due to the fact that the conditional average includes structures at different stages of development, *i.e.* the structures might feature heads that have reached different heights. As discussed above, however, the conditional average clearly includes a structure that is extending further away from the wall (further than 40 viscous units) at a comparably steep angle. For the purpose of identifying a hairpin vortex, it is mainly the fact that the structure clearly extends away from the wall that is important, rather than the presence of a head.

Turbulent Phase

Moving further downstream, we first consider an instantaneous snapshot of the flow at $Re_\theta = 4300$, see Fig. 11. Naturally, the scale separation between inner and outer units is getting larger, and the flow is less and less dominated by large transitional flow structures. As discussed previously, to find a consistent way of automatically educing such vortices is very difficult and not unambiguous, as the educed structures will reflect the specific choice of the eduction scheme. In addition, the span of possible sizes of structures is much larger than at lower Reynolds numbers, which might smear out any potential educed structure. Therefore, in the first step shown here, we take a fundamental approach by discussing three-dimensional visualisations of the vortex cores (*i.e.* connected regions of sufficiently negative λ_2) in the outer region of the layer. As is immediately clear from the visualisations, the dominance of hairpin-like structures is doubtlessly lower than in the previous figures closer to transition, Fig. 9. In this respect it is worth mentioning that one can infer from visualisations (see *e.g.* the animated three-dimensional visualisation of the boundary-layer data [42]) that up to $Re_\theta \approx 1000$ these vortices are still quite frequent, but after $Re_\theta \approx 1500$ their dominance has clearly ceased. This decrease of the hairpin dominance continues to the highest Reynolds number considered in the present study, $Re_\theta = 4300$ as shown in Fig. 11. At this stage, irrespective of the chosen threshold for λ_2, individual hairpins or arches cannot be seen any longer. The boundary layer is now truly turbulent, and the outer layer is dominated by large-scale streamwise alignment of the turbulent vortices, as discussed in the previous sections.

Vortex eduction Having visually established that hairpin vortices are not dominant in the outer part of a boundary layer at sufficiently high Reynolds number, we turn to the question

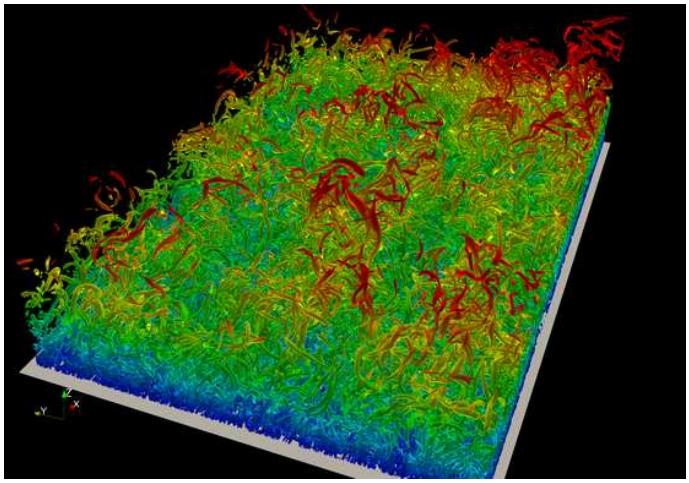

Figure 11: Instantaneous snapshot showing a three-dimensional visualisation of the vortical structures at $Re_\theta = 4300$ (bottom). Isocontours of negative λ_2, coloured by the wall distance. The intermittent structures close to the boundary-layer edge are now clearly visible; they even arrange in large-scale bulges. Contour level: $\lambda_2^+ = -0.001$.

of whether hairpin structures might be more frequent and thus dominant closer to the wall, but hidden by the straightforward visualisations presented so far. Therefore, we make the basic assumption that for a hairpin to exist in the overlap region, say with a spanwise head located about 100-200 viscous units from the wall, smaller hairpin-shaped vortices must exist closer to the wall. These smaller vortices are the seeds of the larger structures as proposed in the auto-generation mechanism advanced by Zhou *et al.* [64] as well as observed and propagated by Wu [58]. Therefore, we can apply the same vortex-eduction scheme discussed above, attempting to educe hairpin vortex structures starting out from their quasi-streamwise legs. The conditional averages, after applying the procedure at two different Reynolds numbers, $Re_\theta = 2500$ and 4200 in the turbulent boundary layer, and at $Re_\tau = 590$ in turbulent channel flow, are shown in Fig. 12 next to each other. In accordance with Jeong *et al.* [19] at lower $Re_\tau = 180$ in channel flow, an isolated, essentially straight vortex tube is educed, with no attached vortex heads. As discussed above it is essential that the local streamwise vorticity component is used for each individual structure to determine the sense of rotation, and the average is constructed after appropriate mirroring of structures, if necessary. It is striking that the educed average coherent wall structures from the different cases are visually indistinguishable, and that the influence of the Reynolds number, scaled in viscous units, is negligible; therefore viscous scaling clearly applies. A more quantitative picture of the geometrical information of the average wall structures, including the sizes and orientations of the structures, has also been collected, not showing significant differences. For the given threshold of λ_2 chosen, an average length is found to be consistently 170 viscous units, and a vortex diameter of about 20 units. No significant Reynolds-number influence can be established from the data.

As noted above, the employed conditional averaging does not account for the very likely situation that the heads of possible hairpins reside at different heights. As a consequence, heads/arches would be smeared out, as partially evident from the conditional average of the educed hairpin vortex in the early transitional region shown in Fig. 10. It was decided to not assume any characteristic details of the hairpins *a priori* (such as vertical scaling *etc.*), and above all preserve the asymmetry of vortical structures which are indeed predominantly found instantaneously here or elsewhere [40, 16, 51, 38]. Therefore, our employed method serves its purpose under

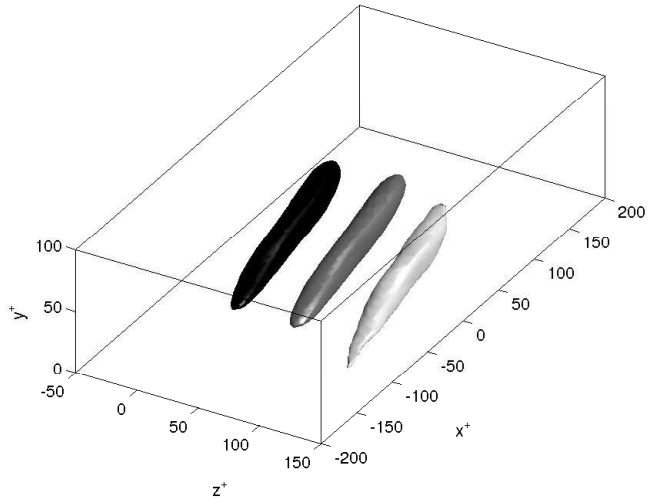

Figure 12: Averaged vortices in the turbulent region, visualised with contour level $\lambda_2^+ = -0.003$. Black: turbulent boundary layer at $Re_\theta = 4200$ ($Re_\tau = 1300$), dark grey: turbulent boundary layer $Re_\theta = 2500$ $Re_\tau = 830$), light grey: turbulent channel $Re_\tau = 590$.

the premise that the conditionally averaged structure does not have to directly yield a complete hairpin structure even in the case hairpins were present the flow. Rather, as is the case for the conditional structure in the low-Re regime, a structure with an upward-oriented "kink" along the streamwise vortex and possibly a smeared vortex head is sufficient. This implies that it is enough to suspect the presence of hairpin vortices if the scheme yields a single streamwise vortex with a kink in the educed structure. However this is not the case for the present data, and the educed structure is very similar to the one already discussed in the earlier channel-flow study [19], which was there connected to the regeneration mechanism in the near-wall region, which does not involve any hairpins [5].

Hairpin vortex signature (HVS)

As discussed in the Introduction, a number of studies have used planar velocity fields, be it from PIV [3, 63] or DNS [26], in an effort to extract structures consistent with the hairpin-vortex model. A vertical slice through the boundary layer reveals ramp-shaped low-speed regions, essentially the LSM. Along these ramps, as summarised by Adrian [1], hairpin-vortex signatures (HVS) are expected: Regions of positive spanwise swirl which signify the heads of larger hairpin vortices whose necks and legs are located on both sides of the vertical plane. Whether both legs are similarly strong is of minor importance for the present discussion.

In the following, we present vertical cuts through the boundary layer, and try to identify similar velocity and vorticity structures as observed in experiments. As previously, two Reynolds numbers are considered; a lower one at $Re_\theta = 1400$ and a higher one at $Re_\theta = 4000$. First consider the visualisations shown in Fig. 13. At this lower Re_θ the boundary-layer thickness is $\delta_{99}^+ \approx 500$. A weak ramp, reaching up to about $y^+ = 200$ can be observed to develop from the wall. Structures identified by negative λ_2 show very strong hairpin vortices, however located at the edge of the boundary layer, *i.e.* around $y = \delta_{99}$. These hairpins are not connected to the ramp-like structure closer to the wall, but rather related to the upstream laminar-turbulent transition, consistent with the earlier discussion.

A vertical cut through the boundary layer at a higher Reynolds number, $Re_\theta = 4000$, is shown

in Fig. 14. Note the striking similarity of this view to Fig. 10 in Ref. [1], both qualitatively and quantitatively. The main feature is a ramp-like low-speed structure extending up to $0.5\delta_{99}$. A number of swirling regions (HVS) are located along the edge of the ramp, highlighted by positive spanwise vorticity. In particular, the signature located slightly downstream of the middle of the figure appears to be a characteristic example of a HVS. Using the numerical data it is possible to plot the complete three-dimensional field around the vertical cut, as done in Fig. 15. The prominent HVS structure indeed corresponds to a strong vortex, positively rotating at the intersection with the vertical plane. The three-dimensional extension however shows that this vortex is not further connected to any structure close to the wall; on one side a short extension in the upstream direction is visible, but even with considerably lowering the threshold for $-\lambda_2$ it does not lead to further elongation into the shape of a hairpin vortex. Based on this figure, and others that were analysed, we can conclude that i) ramp-like large-scale low-speed streaks are indeed visible in agreement with the experimental PIV data, ii) regions of strong positive swirl are grouped along the edges of the ramps in agreement with the concept of hairpin-vortex packets, but iii) the three-dimensional extrapolation of the identified HVS into a (packet of) hairpin(s) does not agree with the three-dimensional picture. On the contrary, and in accordance with concerns raised in Ref. [8], the presented three-dimensional view on vertical planes clearly shows, that "it could be too soon to abandon other, less organized, interpretations", such as the vortex clusters discussed by Ref. [8]. In fact, many of these less organized structures can be identified in the previous visualisations and Fig. 15, and resemble to some extent the tangled filaments and sponges of flakes or strings found in Ref. [8] or the "small-scale, tube-like structures" observed by Pirozzoli [39] of which "very few [...] have shapes conforming to canonical hairpins, such as those found in transitional or post-transitional flows by Wu and Moin".

Conclusions

We have analysed a recent numerical database pertaining to a spatially developing, flat-plate turbulent boundary layer by Schlatter and Örlü [44]. The flow evolves from a laminar Blasius inflow profile, through a transitional patch into an extended region of fully-developed turbulent flow. The Reynolds numbers are unique both in terms of extent, covering $Re_\theta = 180$ to $Re_\theta = 4300$, and simulation setup (including laminar-turbulent transition as in experiments). The main focus is on extracting and assessing the dominant vortical coherent structures in this boundary-layer flow. In particular, the previously found preponderance of clear hairpin vortices, documented by Wu and Moin [59, 60, 61, 58], as well as the call [60] for "further investigation" into "the persistence of the present hairpin forest into higher Reynolds number regions" served as a motivation of the present work, since "evidence for packets at high Reynolds number is less detailed" [29].

In order to provide more quantitative data, we have applied a vortex-eduction method previously proposed and used by Jeong *et al.* [19] in low-Reynolds-number channel flow. This particular method is based on the idea of extracting (quasi-)streamwise vortices in the near-wall region (say up to $y^+ = 40$), and subsequently ensemble averaging to obtain educed structures. Thus, the statistically most dominant near-wall structure can be identified. In channel flow, these structures turned out to be essentially streamwise vortices with slight inclination and tilting. However, there was no associated hairpin head visible in any of the statistical ensembles, clearly indicating that in channel flow the probability of complete hairpin vortices consisting of (streamwise) legs and (spanwise) heads is very rare.

The visual dominance of hairpin vortices in the spatial simulations by Wu and Moin [59] was

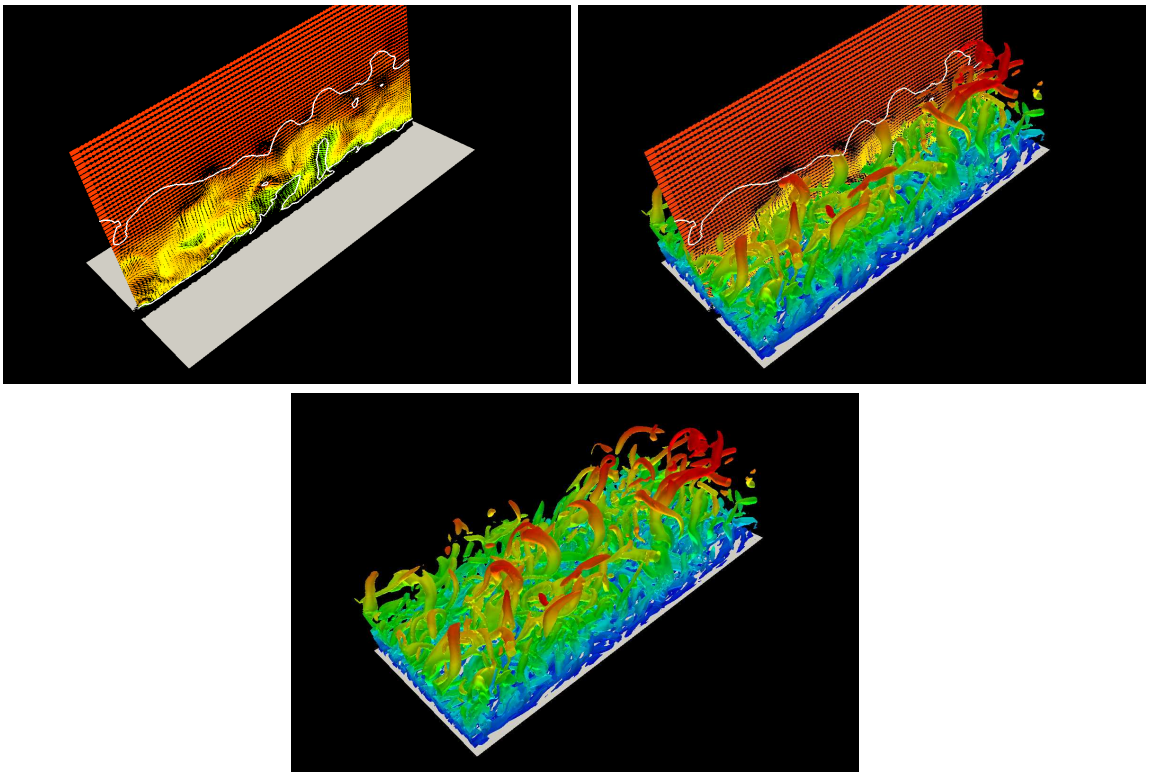

Figure 13: Series of visualisations corresponding to the hairpin-vortex signatures extracted from vertical 2D planes, $Re_\theta \approx 1400$. Mean flow from lower left to upper right; the colour code defines the streamwise velocity magnitude, and the white lines mark $u/U_\infty = 0.99$ and $u/U_\infty = 0.7$, respectively. The vectors show the total in-plane velocity minus 80% of the free-stream velocity U_∞. Vortices are visualised based on λ_2 coloured by wall distance. Natural aspect ratio.

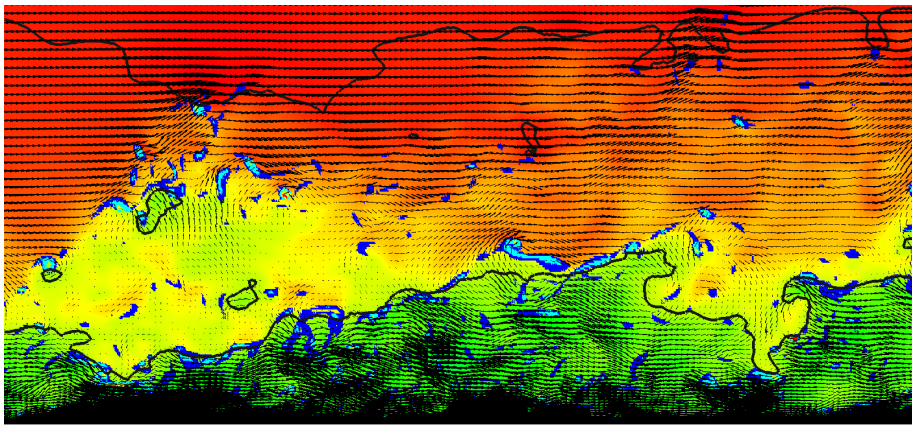

Figure 14: Vertical cut through the boundary layer at $Re_\theta = 4000$ yielding a ramp-shaped pattern. Shown are vectors of the in-plane velocity ($0.75U_\infty$ subtracted). Black lines indicate the location of the instantaneous $u/U_\infty = 0.99$ and $u/U_\infty = 0.7$, respectively. The total in-plane velocity is visualised by the background colour from green to red; blue spots indicate high positive spanwise vorticity events. Natural aspect ratio.

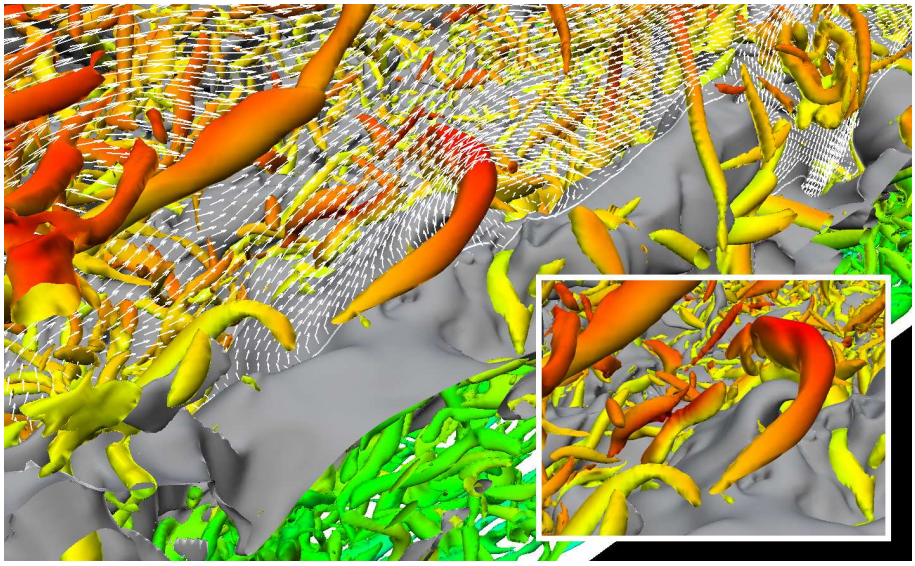

Figure 15: Same snapshot as shown in Fig. 14, but with a three-dimensional representations of the vortical structures. The HVS in the centre corresponds to the characteristic structure located slightly downstream of the middle in Fig. 14. Velocity arrows as in Fig. 14 are shown to facilitate the orientation. The close-up shows a zoomed view of the most probable hairpin-vortex candidate.

indeed remarkable, and possible explanations for the apparent differences between channel and boundary layer were sought in the use of periodic boundary conditions (see *e.g.* Refs. [28, 29]) in most channel simulations. It is therefore important to study a truly spatially evolving boundary layer at comparable Reynolds numbers as in channels. The fact that for the present study we have employed a Fourier method in conjunction with a fringe region cannot at all be compared with a fully periodic setup as in channels, and is therefore of no relevance here: The boundary layer is spatially developing without any residual effects due to the chosen (periodic) discretisation.

Our results show that during the initial development of the boundary layer shortly downstream of the tripping device, hairpin vortices originating from transitional Λ vortices are indeed numerous, and the image of a "forest of hairpins" [60] can be confirmed. The statistical tool based on the eduction method [19] confirms this finding, as the dominant structure at that position is a clear hairpin vortex. This observation is probably not at all surprising, as hairpin-shaped vortices have been known to be dominant structures in various types of transition scenarios including incipient turbulent spots, and are thus very likely to appear at lower Re. Furthermore, at this location along the plate, the scale separation between integral boundary-layer thickness and small-scale turbulence is small so that individual hairpins can actually extend from the wall towards the boundary-layer edge; smaller turbulent scales are virtually absent at that Re indicating that a once generated hairpin vortex does not break-up into smaller scales. Furthermore, several hairpin vortices, when closely spaced, could form a hairpin package and several packages could then merge into a turbulent spot, which is consistent with earlier observations.

However, as Re_θ is increased, the near-wall region does not show any hairpin vortices. Comparing to channel flows, it turns out that even quantitatively no major differences between boundary layers and channels can be detected close to the wall: The educed wall structure is about 200 viscous units in length, and inclined by about 9 degrees. The absence of hairpin vortices in that region and the specific shape of educed structures can be interpreted as an indication that the processes in the near-wall region are not dominated by bursts of varicose (symmetric) type,

but rather of spanwise sinuous type. This agrees with the model based on streak instability by Schoppa and Hussain [47].

In the regions further away from the wall, the identification of hairpin-like structures becomes more difficult, if not more subjective and ambiguous. We have therefore chosen to present a series of different visualisations of these regions. The fact that hairpins are absent in the near-wall cycle is already a strong indication that at least the hypothesis of growing hairpin vortices does not hold. In addition, the visualisations presented herein are also unambiguous in showing that hairpins are seldom found – neither in the near-wall region, in the intermediate overlap region, nor in the outer wake region. These findings are all consistent with observations in channel flows and some previous studies in boundary layers, *e.g.* by Robinson [40].

Motivated by previous experimental studies focusing on the in-plane velocity in a vertical plane, we extracted similar data from our DNS. In agreement with the experiments, inclined ramps reaching up to about $0.5\delta_{99}$ are identified, with regions of high positive swirl grouped along the upper crest. These so-called hairpin-vortex signatures (HVS), essentially positively-rotating spanwise vortices, could also be seen in the DNS. However, the extension of the HSV to three dimensions did not reveal any hairpin legs reaching sufficiently down into the near-wall region.

To summarise, we have documented that i) through vortex eduction the near-wall region is dominated by staggered quasi-streamwise vortices in agreement with theories about sinuous streak breakdown, and ii) at sufficiently high Reynolds number the outer part of the boundary layer does not feature clear hairpin vortices connected to the wall. In particular the latter conclusion is probably not at all unexpected: As the scale separation is increasing, the probability for a large *instantaneous* structure to start at the wall and extend at least to a few hundred viscous units seems low. The present three-dimensional visualisations show a much more random vortical motion in the outer parts, as opposed to the transitional upstream parts.

References

[1] R. J.Adrian Hairpin vortex organization in wall turbulence *Phys. Fluids*, **vol.19**(041301), 2007.

[2] R. J.Adrian and I.Marusic Coherent structures in flow over hydraulic engineering surfaces *J. Hydraul. Res.*, **vol.50**, 451–464, Oct. 2012.

[3] R. J.Adrian, C.Meinhart and C. D.Tomkins Vortex organization in the outer region of the turbulent boundary layer *J. Fluid Mech.*, **vol.422**, 1–54, 2000.

[4] L.Brandt, P.Schlatter and D. S.Henningson Transition in boundary layers subject to free-stream turbulence *J. Fluid Mech.*, **vol.517**, 167–198, 2004.

[5] J.Carlier and M.Stanislas Experimental study of eddy structures in a turbulent boundary layer using particle image velocimetry *J. Fluid Mech.*, **vol.535**, 143–188, 2005.

[6] M.Chevalier, P.Schlatter, A.Lundbladh and D. S.Henningson SIMSON - A Pseudo-Spectral Solver for Incompressible Boundary Layer Flows Technical Report TRITA-MEK 2007:07, KTH Mechanics, Stockholm, Sweden, 2007.

[7] K. T.Christensen and R. J.Adrian Statistical evidence of hairpin vortex packets in wall turbulence *J. Fluid Mech.*, **vol.431**, 433–443, Mar. 2001.

[8] J. C.Del Álamo, J.Jiménez, P.Zandonade and R. D.Moser Self-similar vortex clusters in the turbulent logarithmic region *J. Fluid Mech.*, **vol.561**, 329–358, Aug. 2006.

[9] G. E.Elsinga, R. J.Adrian, B. W.van Oudheusden and F.Scarano Three-dimensional vortex organization in a high-Reynolds-number supersonic turbulent boundary layer *J. Fluid Mech.*, **vol.644**, 35–60, Feb. 2010.

[10] B.Ganapathisubramani, N.Hutchins, W. T.Hambleton, E. K.Longmire and I.Marusic Investigation of large-scale coherence in a turbulent boundary layer using two-point correlations *J. Fluid Mech.*, **vol.524**, 57–80, 2005.

[11] Y. G.Guezennec, U.Piomelli and J.Kim On the shape and dynamics of wall structures in turbulent channel flow *Phys. Fluids A*, **vol.1**, 764–766, 1989.

[12] J. M.Hamilton, J.Kim and F.Waleffe Regeneration mechanisms of near-wall turbulence structures *J. Fluid Mech.*, **vol.287**, 317–348, 1995.

[13] M. R.Head and P.Bandyopadhyay New aspects of turbulent boundary-layer structure *J. Fluid Mech.*, **vol.107**, 297–338, 1981.

[14] S. E.Hommema and R. J.Adrian Packet structure of surface eddies in the atmospheric boundary layer *Bound.-Lay. Meteorol.*, **vol.106**, 147–170, 2003.

[15] S.Hoyas and J.Jiménez Scaling of the velocity fluctuations in turbulent channels up to $Re_\tau = 2003$ *Phys. Fluids*, **vol.18**(011702), 2006.

[16] N.Hutchins, W. T.Hambleton and I.Marusic Inclined cross-stream stereo particle image velocimetry measurements in turbulent boundary layers *J. Fluid Mech.*, **vol.541**, 21–54, Oct. 2005.

[17] N.Hutchins and I.Marusic Large-scale influences in near-wall turbulence *Phil. Trans. R. Lond. Soc. A*, **vol.365**, 647–664, 2007.

[18] J.Jeong and F.Hussain On the identification of a vortex *J. Fluid Mech.*, **vol.285**, 69–94, 1995.

[19] J.Jeong, F.Hussain, W.Schoppa and J.Kim Coherent structures near the wall in a turbulent channel flow *J. Fluid Mech.*, **vol.332**, 185–214, 1997.

[20] J.Jiménez, S.Hoyas, M. P.Simens and Y.Mizuno Turbulent boundary layers and channels at moderate Reynolds numbers *J. Fluid Mech.*, **vol.657**, 335–360, 2010.

[21] A. V.Johansson, P. H.Alfredsson and J.Kim Evolution and dynamics of shear-layer structures in near-wall turbulence *J. Fluid Mech.*, **vol.224**, 579–599, 1991.

[22] K. C.Kim and R. J.Adrian Very large-scale motion in the outer layer *Phys. Fluids*, **vol.11**, 417–422, 1999.

[23] J. C.Klewicki Reynolds number dependence, scaling and dynamics of turbulent boundary layers *J. Fluids Eng.*, **vol.132**(094001), 2010.

[24] J. C.Klewicki, M. M.Metzger, E.Kelner and E.Thurlow Viscous sublayer flow visualizations at R=1500000 *Phys. Fluids*, **vol.7**, 867–863, 1995.

[25] S. J.Kline, W. C.Reynolds, F. A.Schraub and P. W.Runstadler The structure of turbulent boundary layers *J. Fluid Mech.*, **vol.30**, 741–773, 1967.

[26] J. H.Lee and H. J.Sung Very-large-scale motions in a turbulent boundary layer *J. Fluid Mech.*, **vol.673**, 80–120, Feb. 2011.

[27] P.Lenaers, Q.Li, G.Brethouwer, P.Schlatter and R.Örlü Rare backflow and extreme wall-normal velocity fluctuations in near-wall turbulence *Phys. Fluids*, **vol.24**, 035110, 2012.

[28] I.Marusic Unravelling turbulence near walls *J. Fluid Mech.*, **vol.630**, 1–4, 2009.

[29] I.Marusic and R. J.Adrian The Eddies and Scales of Wall Turbulence *Wall Turbulent Flows, ed. P. Davidson, K. R. Sreenivassan, CUP*, pages 1–46, Nov. 2013.

[30] I.Marusic, B. J.McKeon, P. A.Monkewitz, H. M.Nagib, A. J.Smits and K. R.Sreenivasan Wall-bounded turbulent flows at high reynolds numbers: Recent advances and key issues *Phys. Fluids*, **vol.22**(065103), 2010.

[31] S. C.Morris, S. R.Stolpa, P. E.Slaboch and J. C.Klewicki Near-surface particle image velocimetry measurements in a transitionally rough-wall atmospheric boundary layer *J. Fluid Mech.*, **vol.580**, 319–338, 2007.

[32] C.O'Farrell and M. P.Martín Chasing eddies and their wall signature in DNS data of turbulent boundary layers *J. Turbulence*, **vol.10**(15), 1–22, 2009.

[33] R.Örlü *Experimental studies in jet flows and zero pressure-gradient turbulent boundary layers* PhD thesis, Department of Mechanics, KTH Stockholm, Sweden, 2009.

[34] R.Örlü and P.Schlatter On the fluctuating wall-shear stress in zero-pressure-gradient turbulent boundary layer flows *Phys. Fluids*, **vol.23**(021704), 2011.

[35] R.Örlü and P.Schlatter Turbulent boundary layer flow: comparing experiments with DNS In M.Oberlack, J.Peinke, A.Talamelli, L.Castillo and M.Höllig, editors, *Progress in Turbulence and Wind Energy IV*, pages 213–216, 2012.

[36] R. L.Panton Overview of the self-sustaining mechanisms of wall turbulence *Prog. Aero. Sci.*, **vol.37**, 341–383, 2001.

[37] A. E.Perry and M. S.Chong On the mechanism of wall turbulence *J. Fluid Mech.*, **vol.119**, 173–217, 1982.

[38] S.Pirozzoli Flow organization near shear layers in turbulent wall-bounded flows *J. Turbulence*, **vol.12**, N41, 2011.

[39] S.Pirozzoli and M.Bernardini Turbulence in supersonic boundary layers at moderate Reynolds number *J. Fluid Mech.*, **vol.688**, 120–168, 2011.

[40] S. K.Robinson Coherent motions in the turbulent boundary layer *Annu. Rev. Fluid Mech.*, **vol.23**, 601–639, 1991.

[41] N. D.Sandham and L.Kleiser The late stages of transition to turbulence in channel flow *J. Fluid Mech.*, **vol.245**, 319–348, 1992.

[42] P.Schlatter, M.Chevalier, M.Ilak and D. S.Henningson The structure of a turbulent boundary layer studied by numerical simulation *arXiv*, **vol.1010.4000**, 2010 (including animation).

[43] P.Schlatter, Q.Li, G.Brethouwer, A. V.Johansson and D. S.Henningson Simulations of spatially evolving turbulent boundary layers up to $Re_\theta = 4300$ *Int. J. Heat Fluid Flow*, **vol.31**, 251–261, 2010.

[44] P.Schlatter and R.Örlü Assessment of direct numerical simulation data of turbulent boundary layers *J. Fluid Mech.*, **vol.659**, 116–126, 2010.

[45] P.Schlatter and R.Örlü Turbulent boundary layers at moderate Reynolds numbers. Inflow length and tripping effects *J. Fluid Mech.*, **vol.710**, 5–34, 2012.

[46] P.Schlatter, R.Örlü, Q.Li, G.Brethouwer, J. H. M.Fransson, A. V.Johansson, P. H.Alfredsson and D. S.Henningson Turbulent boundary layers up to $Re_\theta = 2500$ studied through numerical simulation and experiments *Phys. Fluids*, **vol.21**(051702), 2009.

[47] W.Schoppa and F.Hussain Coherent structure generation in near-wall turbulence *J. Fluid Mech.*, **vol.453**, 57–108, 2002.

[48] A.Schröder, R.Geisler, K.Staack, G. E.Elsinga, F.Scarano, B.Wieneke, A.Henning, C.Poelma and J.Westerweel Eulerian and Lagrangian views of a turbulent boundary layer flow using time-resolved tomographic PIV *Exp. Fluids*, **vol.50**, 1071–1091, Dec. 2011.

[49] A. J.Smits, B. J.McKeon and I.Marusic High-Rreynolds number wall turbulence *Annu. Rev. Fluid Mech.*, **vol.43**, 353–375, 2011.

[50] P. R.Spalart Direct simulation of a turbulent boundary layer up to $R_\theta = 1410$ *J. Fluid Mech.*, **vol.187**, 61–98, 1988.

[51] M.Stanislas, L.Perret and J. M.Foucaut Vortical structures in the turbulent boundary layer: a possible route to a universal representation *J. Fluid Mech.*, **vol.602**, 327–382, Apr. 2008.

[52] T.Theodorsen The Structure of Turbulence 50 Jahre Grenzschichtforschung, edited by H. Görtler and W. Tollmien. Friedrich Vieweg & Sohn, Braunschweig., 1955.

[53] A.Thomas and M.Bull On the role of wall-pressure fluctuations in deterministic motions in the turbulent boundary layer *J. Fluid Mech.*, **vol.128**, 283–322, 1983.

[54] C. D.Tomkins and R. J.Adrian Spanwise structure and scale growth in turbulent boundary layers *J. Fluid Mech.*, **vol.490**, 37–74, 2003.

[55] A. A.Townsend The structure of turbulent shear flow *Cambridge University Press, 2nd ed.*, 1976.

[56] F.Waleffe On a self-sustaining process in shear flows *Phys. Fluids*, **vol.9**, 883–900, 1997.

[57] J. M.Wallace Highlights from 50 years of turbulent boundary layer research *J. Turbulence*, **vol.13**(53), 1–71, 2012.

[58] X.Wu Establishing the generality of three phenomena using a boundary layer with free-stream passing wakes *J. Fluid Mech.*, **vol.664**, 193–219, 2010.

[59] X.Wu and P.Moin Direct numerical simulation of turbulence in a nominally zero-pressure-gradient flat-plate boundary layer *J. Fluid Mech.*, **vol.630**, 5–41, 2009.

[60] X.Wu and P.Moin Forest of hairpins in a low-Reynolds-number zero-pressure-gradient flat-plate boundary layer *Phys. Fluids*, **vol.21**, 091106, 2009.

[61] X.Wu and P.Moin Transitional and turbulent boundary layer with heat transfer *Phys. Fluids*, **vol.22**, 085105, 2010.

[62] X.Wu and P.Moin Evidence for the Persistence of Hairpin Forest in Turbulent, Zero-pressure-gradient Flat-plate Boundary Layers *Proc. 7th Intl Symp. on Turbulence and Shear Flow Phenomena, Ontario, Canada*, pages 1–6, Apr. 2011.

[63] Y.Wu and K. T.Christensen Spatial structure of a turbulent boundary layer with irregular surface roughness *J. Fluid Mech.*, **vol.655**, 380–418, 2010.

[64] J.Zhou, R. J.Adrian, S.Balachandar and T. M.Kendall Mechanisms for generating coherent packets of hairpin vortices in channel flow *J. Fluid Mech.*, **vol.387**, 353–396, 1999.